Title

Investigations on T cell transmigration in a human skin-on-chip (SoC) model

Journal

Lab on a Chip, 21(8)

ISSN

1473-0197

Authors

Ren, Xiaoou

Getschman, Anthony E

Hwang, Samuel

et al.

Publication Date

2021-04-20

DOI

10.1039/d0lc01194k

Peer reviewed

ARTICLE

Investigations on T Cell Transmigration in a Human Skin-on-Chip (SoC) Model

Received 00th January 20xx,
Accepted 00th January 20xx

DOI: 10.1039/x0xx00000x

Xiaoou Ren[ab], Anthony E. Getschman[c], Samuel Hwang[d], Brian F. Volkman[c], Thomas Klonisch[e], David Levin[b], Min Zhao[d], Susy Santos[f], Song Liu[b], Jasmine Cheng[a] and Francis Lin[abdg*]

A microfluidics-based three-dimensional skin-on-chip (SoC) model is developed in this study to enable quantitative studies of transendothelial and transepithelial migration of human T lymphocytes in mimicked skin inflammatory microenvironments and to test new drug candidates. The keys results include 1) CCL20-dependent T cell transmigration is significantly inhibited by an engineered CCL20 locked dimer (CCL20LD), supporting the potential immunotherapeutic use of CCL20LD for treating skin diseases such as psoriasis; 2) transepithelial migration of T cells in response to a CXCL12 gradient mimicking T cell egress from the skin is significantly reduced by a Sphingosine-1-phosphate (S1P) background, suggesting the role of S1P for T cell retention in inflamed skin tissues; and 3) T cell transmigration is induced by inflammatory cytokine stimulated epithelial cells in the SoC model. Collectively, the developed SoC model recreates a dynamic multi-cellular micro-environment that enables quantitative studies of T cell transmigration at a single cell level in response to physiological cutaneous inflammatory mediators and potential drugs.

Introduction

T cell migration is a critical process that plays an essential great role in immune responses.[1] The migratory behavior of T cells is induced by specific chemokines through multiple chemotactic signaling transduction pathways. The chemotactic T cell responses enable rapid cell movement through a complex physiological environment to effect rapid and direct immune surveillance toward foreign antigenic challenge at inflammatory sites.[2-7] Upon activation, T cell migration from the lymph nodes to inflammatory skin sites via the bloodstream is controlled by multiple interactions between different "homing" receptors and their respective ligands.[8] Detailed studies have demonstrated that T cell migration is involved in the psoriatic pathogenesis, and can modulate the extent of psoriatic inflammatory processes.[9, 10] T cell migration is also closely associated with other various skin diseases, including vitiligo, atopic dermatitis, and alopecia areata.[11-13] Collectively, T cell migration is important for maintaining skin homeostasis with high relevance to skin diseases.

Human skin is the largest organ of the human body, provides a vital protective barrier function and consists of the three major layers: outermost epidermis, dermis, and hypodermis (**Figure 1A**).[14-16] The epidermis contains keratinocytes at various stages of differentiation with a regenerative stratum adjacent to the basement membrane, which separates the epidermal from the dermal layer. Dermis and hypodermis consist of fibroblasts that synthesize extracellular matrix (ECM), of which collagen is the most abundant component, to maintain the structural integrity of the tissue and vascular networks.[16, 17] Skin inflammatory processes trigger T cells trafficking to regional lymph nodes and this involves down-regulation of the C-C motif chemokine receptor 7 (CCR7)/ C-C motif chemokine ligand 21 and 19 (CCL21/19) axis. In contrast, the C-C motif chemokine receptor 6 (CCR6)/ C-C motif chemokine ligand 20 (CCL20) system is up-regulated in the dermis and epidermis and this facilitates T cell homing to the inflammatory site.[8] In psoriatic skin lesions, CCR6/ CCL20 signaling facilitates inflammatory processes by promoting the migration and accumulation of T cells at psoriasiform sites. This CCR6-mediated T cell migration can be inhibited by an engineered CCL20 locked dimer (CCL20LD).[18] Other studies reported the C-X-C motif chemokine receptor 4 (CXCR4)/ C-X-C motif chemokine ligand 12 (CXCL12) (i.e., stromal cell-derived factor-1 alpha (SDF-1α)) ligand-receptor system being up-regulated during skin inflammation and

[a] Department of Physics and Astronomy, University of Manitoba, Winnipeg, MB, R3T 2N2, Canada.
[b] Department of Biosystems Engineering, University of Manitoba, Winnipeg, MB, R3T 2N2, Canada.
[c] Department of Biochemistry, Medical College of Wisconsin, Milwaukee, WI, 53226, USA
[d] Department of Dermatology, University of California Davis School of Medicine, Sacramento, CA, 95816, USA
[e] Department of Human Anatomy and Cell Science, University of Manitoba, Winnipeg, MB, R3E 0J9, Canada
[f] Victoria General Hospital, Winnipeg, MB, R3T 2E8, Canada.
[g] Department of Immunology, University of Manitoba, Winnipeg, MB, R3E 0T5, Canada.
*Address for correspondence: Francis Lin, Department of Physics and Astronomy, University of Manitoba, 30A Sifton Rd, 301 Allen Bldg, Winnipeg, MB, R3T 2N2, Canada. flin@physics.umanitoba.ca

Electronic Supplementary Information (ESI) available. See DOI: 10.1039/x0xx00000x

contributing to inflammatory angiogenesis.[19-21] In addition, the up-regulation of the sphingosine-1-phosphate receptor 1 (S1PR1)/ Sphingosine-1-phosphate (S1P) axis in inflamed peripheral tissues, including skin and blood vessels, and the high expression of S1P at the inflammatory sites has been linked to T cell retention at these sites.[22] Hence, the regulation of T cell trafficking in the skin is orchestrated by complex mechanisms controlled by chemical fields that are subject to dynamic changes during inflammation (**Figure 1B-C**).

Microfluidic devices provide an advanced platform to mimic physiological conditions for biological and biomedical research and this field of research has been fast growing in recent years.[23, 24] This technology is well suited for cell migration studies owing to key advantages of microfluidics, such as miniaturization, precise and flexible chemical gradient generation, low reagent consumption, and high-throughput experimentation.[25-28] Despite these advantages, the majority of microfluidic devices used for cell migration studies suffer from several limitations. These drawbacks include the reconstitution of much-simplified stable chemical fields, ECM, and single cell type based microenvironments, which do not reflect the complex *in-vivo* microenvironment cells encounter during their tissue migration.[29] The "organ-on-chip" microfluidic devices are an attractive new modification which structurally integrate cell co-culture strategies in the microfluidics design to better simulate the key activities and responses of certain tissues or organs.[29] Among them are "liver-on-a-chip", "kidney-on-a-chip", "muscle-on-a-chip", and "lymph node-on-a-chip".[30-34] A recent study demonstrated the feasibility of constructing a mimetic "skin-on-chip" (SoC) model *in vitro*, which was used for drug toxicity testing and disease studies.[35] However, no study has applied a SoC model for T cell migration studies. This motivated us to develop such an approach for investigating cutaneous T cell migration in a reconstituted *in-vivo* microenvironment based on a microfluidic device specifically designed for this purpose.

In this study, we have developed a novel microfluidic SoC model (**Figure S1**) that resembles key features of the human skin. For the first time, we used this SoC model to study T cell migratory responses towards the effects of controlled complex

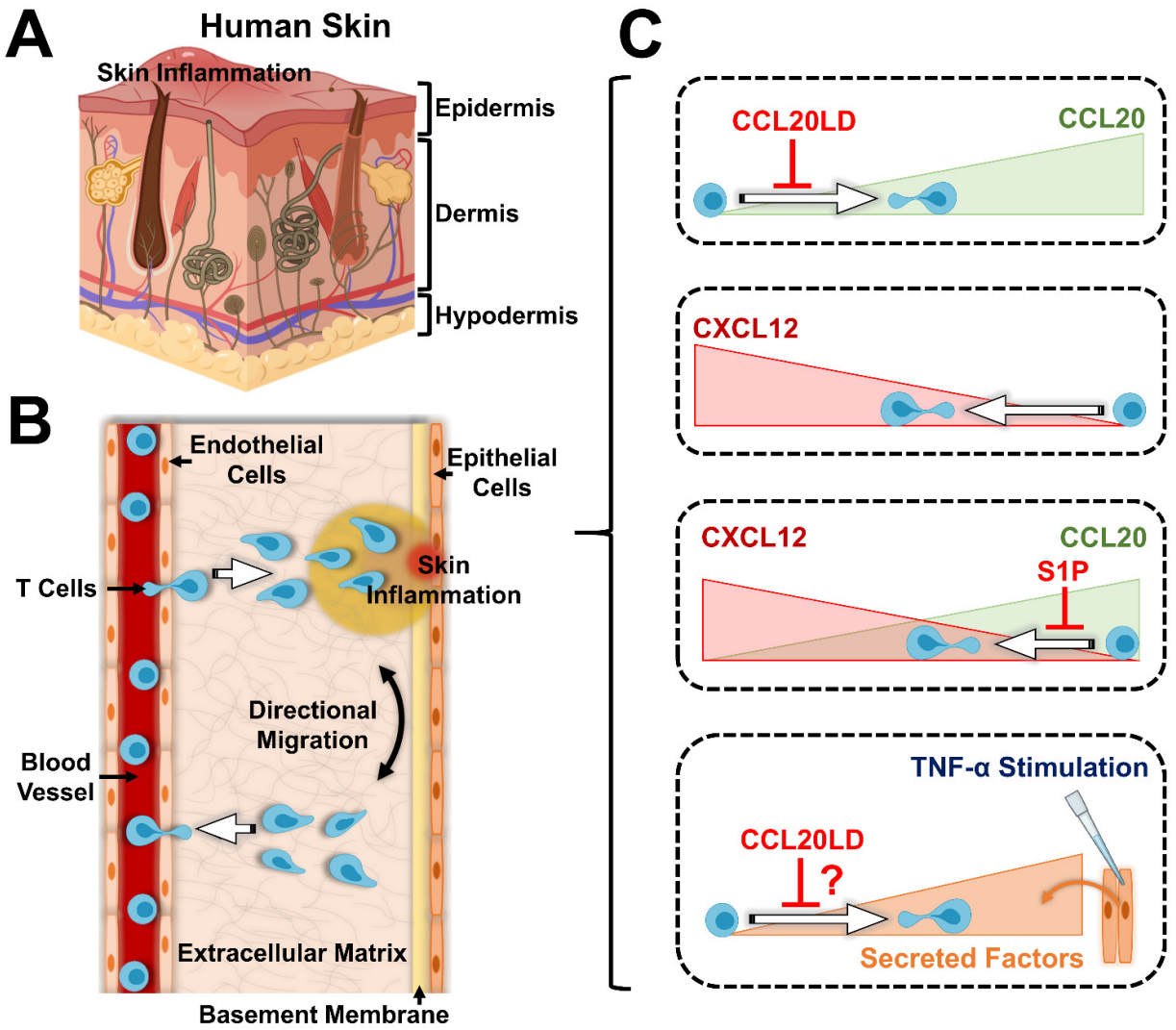

Figure 1. Illustration of the inflamed human skin, T cell transmigration in inflamed human skin, and T cell transmigration in different chemokine fields in the skin-on-chip (SoC) model. (A) Schematic illustration of basic histological structure of the human skin. **(B)** Illustration of transendothelial extravasation of blood-derived T cells during skin inflammation. **(C)** Schematic illustration of the effects of different chemokine fields on T cell transmigration in the SoC model.

chemical gradients simulating cutaneous inflammation. Our microfluidic device (**Figure S1A**) enabled performance measurements of four parallel cell migration experiments simultaneously conducted by four identical independent units, each independently controlling gradient generation. This SoC model was compatible with different immune cell types, including activated human peripheral blood T cells (ahPBTs) and human blood neutrophils (**Figure S2**). Each unit consists of one gel channel, with one gel inlet (1 mm diameter) and one gel well (3 mm diameter) flanked by two side channels with two chemical inlets (1 mm diameter) and two chemical wells (6 mm diameter) (**Figure S1B**). The smaller sized gel and chemical inlets provide better sealing when solutions are loaded. The front portion length of the gel channel (5000 µm) is longer than the major compartment (1140 µm) and the back portion (3000 µm) to reduce the initial flow speed of gel solution. Although the method of patterning gel in the device using micropillars is similar to other studies,[36-39] the number, layout and dimension of the micropillars was designed and modified in a more compact manner (**Figure S1C**).

Specifically, the major compartment is divided by four trapezoidal micropillars to provide multiple view regions for the cell migration experiments. The gap (120 µm) between two neighboring micropillars provides enough space to allow sufficient T cells to migrate across the gap simultaneously. The design of micropillars conducted with hydrophobicity restoration of PDMS enabled the selective gel patterning in the major compartment (**Figure 2A-B**). Establishment of the HaCaT cell layer, three dimensional (3D) collagen gel with porous fiber structure, and HUVEC cell layer in the device replicated major features of the epithelium, ECM, and endothelium *in vitro* (**Figure 2B-D)**. In addition, the ratio of width of the gel compartment (500 µm) to the thickness of a few cell layers of HaCaT (~tens of microns) was designed to reflect the *in-vivo* ratio of dermis to epidermis (approximately 3-60 folds).[40, 41] A single or competing gradient (**Figure 2E-F)** of relevant chemokines was generated based on the chemical diffusion from one side channel to the other through the collagen gel to mimic the *in-vivo* chemical fields during skin inflammation. We demonstrated the application of this SoC model for simulating on-chip skin inflammation using tumor necrosis factor-α (TNF-α) stimulation. Furthermore, we used a previously engineered CCL20LD to successfully inhibit CCR6-mediated T cell migration in our SoC model. Our results demonstrate the capability and potential of this SoC model to investigate the role of physiologically relevant chemical fields in mediating cutaneous T cell homing and may serve as a novel drug screening platform to identify compounds targeting skin diseases (e.g., psoriasis).

Materials and methods

Collection of blood samples

An ethics protocol (J2015:022) was approved by the Joint-Faculty Research Ethics Board at the University of Manitoba for collecting blood samples from healthy human donors. All

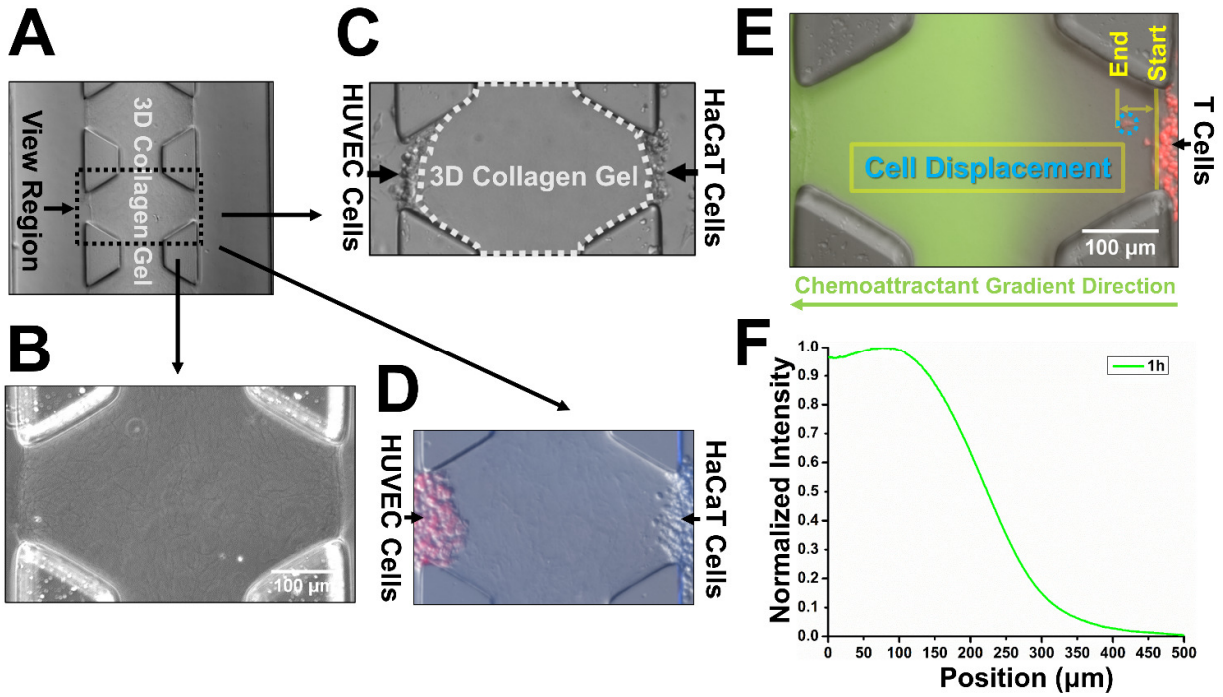

Figure 2. Illustration of the 3D collagen gel formation, HUVEC/ HaCaT cell patterning, cell displacement analysis, and FITC-Dextran gradient profile plot in the micropillar device. (A) Representative image showing the 3D collagen gel matrix in the middle gel channel of the device. The black dashed box shows one field of view under the microscope. **(B)** A representative phase-contrast image of the selected field of view region from Figure A shows the ECM filled space upon gelation in the magnified viewing area (scale bar: 100 µm). **(C-D)** Representative DIC and fluorescent images of the selected field of view from Figure A show the 3D gel with HUVEC/ HaCaT cell patterning in the device. The white dashed box shows the 3D collagen gel with adherent HUVEC (left side) and HaCaT cells (right side) in Figure C; the red and blue colored dots indicate the HUVEC and HaCaT cells, respectively, attached to both sides of the 3D collagen gel in Figure D. **(E)** A representative fluorescent image of the selected field of view region from Figure A illustrates cell migration displacement analysis (scale bar: 100 µm). The red colored dots indicate labeled T cells, and the green color in the channel indicates the profile and most concentrated area of the chemical gradient. **(F)** Representative fluorescence intensity plot displaying the chemical gradient at 1 hour (1h) of experimentation in this device.

the participants were recruited at the Victoria General Hospital (Winnipeg, Manitoba, Canada) according to the approved procedures. Specifically, each participant reviewed a consent form in detail and discussed any concerns or questions with the recruiting staff prior to consenting. Peripheral blood samples were then collected from these consented healthy donors at the hospital.

Preparation of activated human peripheral blood T cells

Human peripheral blood samples were obtained from healthy donors according to the mentioned procedures. A standard gradient centrifugation method was conducted for isolating peripheral blood mononuclear cells (PBMCs) from the blood samples. T cells within the PBMCs were selectively activated by adding anti-human CD3 (Purified anti-human CD3 Antibody, BioLegend, catalog# 300302) and anti-human CD28 (Purified anti-human CD28 Antibody, BioLegend, catalog# 302901) antibodies at a final concentration of 1 µg/ml for each in complete RPMI-1640 culture medium (RPMI-1640 with 1% penicillin-streptomycin and 10% FBS) for 2 days inside an incubator (37 °C, 5% CO_2). The ahPBTs proliferated in the same culture medium with a supplement of 12.5 ng/ml of interleukin-2 (IL-2) (R&D Systems) for at least 3 days before the start of the cell migration experiments.[6, 25, 42]

Preparation of human blood neutrophils

Human blood neutrophils were isolated from the peripheral blood samples of healthy donors using a magnetic negative selection kit (EasySep Direct Human Neutrophil Isolation Kit, STEMCELL). The isolated neutrophils were cultured in the complete RPMI-1640 culture medium (RPMI-1640 with 1% penicillin-streptomycin and 10% FBS) in an incubator (37°C, 5% CO_2) and used for cell migration experiments within 8 h of isolation.

Cell culture

Human immortalized keratinocytes (HaCaT) were provided by Dr. Song Liu through his collaboration with Dr. Aziz Ghahary at the University of British Columbia. Human umbilical vein endothelial cells (HUVEC) were provided by Dr. Min Zhao purchased from ATCC. HaCaT and HUVEC cells were used as substitutes to represent cellular components of the epithelium and blood vessel compartment in the skin, respectively.[35] HaCaT and HUVEC cells were cultured in complete DME/F12 culture medium (DME/F12 with 1% penicillin-streptomycin and 10% FBS) in an incubator (37 °C, 5% CO_2) prior cell migration experiments.

Cell labeling

The CellTracker™ fluorescent probes Orange CMRA Dye (C34551) and Violet BMQC Dye (C10094) (both Molecular Probes, Invitrogen) were used to label cells and to demonstrate the positions of the labelled cells. Cell labeling was conducted according to the manufacturer's protocol. Cells were collected from the culture medium and incubated with pre-warmed (37 °C) CellTracker™ working solution (0.5 µM) in serum-free medium for 45 minutes inside an incubator (37 °C, 5% CO_2). The labelled cells were then extracted from the CellTracker™ working solution and re-suspended in the culture medium before cell migration experiments.

Fabrication of the microfluidic device

The device pattern was designed in SolidWorks® (ver. 2012, Dassault Systems S.A.), and fabricated on a three inch silicon wafer (Silicon, Inc., ID) using standard photolithography methods.[43-45] The fabrication process and dimension measurements were conducted in our lab at the Department of Physics and Astronomy and the Nano Systems Fabrication Laboratory at the University of Manitoba, respectively. Briefly, the designed pattern was printed onto a transparent film at 24,000 dpi resolution (Fineline Imaging, Colorado Springs, CO) and replicated onto a silicon wafer with pre-coated SU-8 negative photoresist (MicroChem Corporation, Westborough, MA) using selective ultraviolet exposure of the film. The patterned wafer served as the mold to reproduce polydimethylsiloxane (PDMS) (Sylgard 184, Dow Corning, Manufacturer SKU# 2065622) replicas using standard soft-lithography methods.[43-45] Specifically, the PDMS working solution was prepared by mixing PDMS and its curing agent at the ratio of 10: 1 (w/w), followed by pouring the solution into the mold. The PDMS replica was cut off from the mold after 2h of baking at 80 °C in an oven. The gel inlet, gel well, chemical inlets, and chemical wells were punched out of the PDMS replica, followed by bonding the replica onto a glass slide using an air plasma cleaner (Harrick Plasma, Ithaca, NY).

Preparations of ECM and cell layers in the device

The device was baked in the oven overnight to restore the hydrophobicity before gel loading. This process has been commonly applied by others to prevent gel leakage.[36, 37, 39] As collagen is the most abundant component in the human dermal ECM,[16, 17] RatCol® Rat Tail Collagen Kit (catalog# 5153, Advanced BioMatrix, San Diego, CA) was used as 3D hydrogels to mimic the *in-vivo* ECM with porous fiber structure.[46, 47] Type I rat tail collagen solution (3.8 mg/ml) from the kit was gently mixed with its neutralization solution at the ratio of 9: 1 (v/v) according to the manufacturer's protocol, followed by a second dilution step with phosphate buffer saline (PBS, 1×) at the ratio of 1: 1 (v/v) in a pre-cooled (-20 °C) Eppendorf tube. The diluted mixture was injected into the gel inlet to fully fill the gel channel, and the gel well was filled up. All the procedures including 3D collagen gel preparation and injection were conducted on ice to prevent uncontrolled gelation. The device was then placed in the incubator for 30 minutes of gelation. The porous fiber structure of the 3D collagen gel was visualized in the gel channel, without any leakage occurring to the side channels (**Figure 2B**). For surface coating, collagen at 20 µg/mL was gently injected from the chemical inlets to fully fill the chemical channel and the device was incubated for 1h in the incubator. Upon removal of the coating solution, each chemical well was injected with complete DME/F-12 culture medium, and the device was transferred to the incubator for

30 minutes before the medium inside the chemical wells was discarded. HaCaT and HUVEC cell solutions (1× 10^5 cells in 100 µL/well) were loaded into the chemical wells drop by drop and the device was returned to the incubator to allow the attachments of HaCaT and HUVEC cells to both sides of the collagen gel. HaCaT and HUVEC cell layers had formed after 2h of incubation (**Figure 2C-D**). The device was kept inside the incubator overnight prior to cell migration experiments. The device was placed inside a humidified chamber (i.e., a pipette tip box with damp tissues on the rack and small volumes of deionized water in the bottom chamber) during all incubation procedures to prevent drying of samples. When testing cell migration with collagen gel alone, the identical procedure was conducted, but with the omission of loading HaCaT and HUVEC cells, and the device was incubated with complete DME/F-12 culture medium in the incubator overnight. On-chip stimulation with TNF-α used the same procedure but the incubation time with HaCaT and HUVEC cells was 2h and the medium was discarded from the chemical wells before treatment.

Preparation of the chemoattractants

Complete DME/F-12 culture medium was used to culture HaCaT and HUVEC cells and served as medium control and diluent. CXCL12 at the concentration of 100 ng/mL,[42] was used as positive control in the experiments involving migration of T cells through the HaCaT/ collagen gel layers. CCL20 wild-type (WT) was synthesized as previously described,[18] and prepared at a concentration of 100 ng/mL as positive control for those experiments that investigated T cell migration through HUVEC/ collagen gel layers. In some experiments, a competing CCL20WT/ CXCL12 gradient with or without a uniform background of 100 ng/mL of S1P was generated to test migration of T cells through the HaCaT/ collagen gel layers in the SoC device. A previously engineered CCL20LD,[18] was prepared at concentrations of 100 ng/mL and 1.6 µg/mL and used as an inhibitor to CCR6-mediated T cell migration.

TNF-α induced skin inflammation in the device

The well-known inflammatory mediator TNF-α was prepared at the concentration of 100 ng/mL,[35] to simulate skin inflammation *in vitro* in the microfluidic device. TNF-α solution (100 µL) and complete DME/F-12 culture medium (100 µL) were injected in the chemical well at the HaCaT and HUVEC side, respectively, for overnight incubation. The next day, supernatants from the chemical well at the HUVEC side were discarded, whereas the supernatants from the chemical well at the HaCaT side were collected. Any remaining HaCaT cells in the supernatants were removed by centrifugation prior to using these supernatants as chemoattractant solutions for the T cell migration experiments. The chemical wells were incubated with complete DME/F-12 culture medium (100 µL/well) in the incubator before commencing cell migration experiments.

Setup of the cell migration experiments

Prior to the start of cell migration experiments, complete DME/F-12 culture medium remaining in the chemical wells was discarded. The ahPBTs were extracted and re-suspended in complete DME/F-12 culture medium before loading into the device. Fluorescein isothiocyanate (FITC)-dextran (10 kDa, final concentration of 5 µM, Sigma-Aldrich, Catalog# FD10S) was added into all the chemoattractant solutions (e.g., CXCL12, CCL20WT, CCL20LD, and supernatants), except the competing gradient experiments, to characterize the chemical gradient in real time.[42, 44] One chemical well was loaded with T cells (1× 10^5 cells in 100 µL) first and T cells were allowed to attach to the collagen gel or HaCaT/ HUVEC cell layers for several minutes. This was followed by loading the chemoattractant solution (100 µL) into the other chemical well to generate the chemical gradient. All loading procedures were conducted drop by drop to prevent damage to the collagen gel. The loaded device was placed on a movable stage under an inverted fluorescence microscope (Nikon Ti-U) inside an environmental controlled chamber (InVivo Scientific) at 37 °C during the experiment. Differential interference contrast (DIC) images during cell migration experiments were taken at multiple positions at 0h, 0.5h and 1h, respectively, for each device. When not taking images, the device was incubated inside the humidified chamber in the incubator.

Data analysis

All experimental conditions were independently replicated at least three times. The DIC images of cell migration were extracted from the NIS Element Viewer (Nikon) and analyzed with ImageJ software (NIH). Cells that transmigrated through the collagen gel and/or HaCaT/ HUVEC cell layers from the boundary towards the most concentrated area of the gradient inside the channel were recorded within the microscopic field of view. The directional cell migration displacement (**Figure 2E**) towards the gradient direction was recorded for individual T cells during the experiment. The OriginPro software was used for statistical analysis of the data presented in the Box Chart. Two-sample Student's t-test was conducted to compare different conditions, and *$p < 0.05$, **$p < 0.01$ and ***$p < 0.001$ were indicated statistically significant difference.

Results

SoC model validation with CXCL12 induced T cell migration

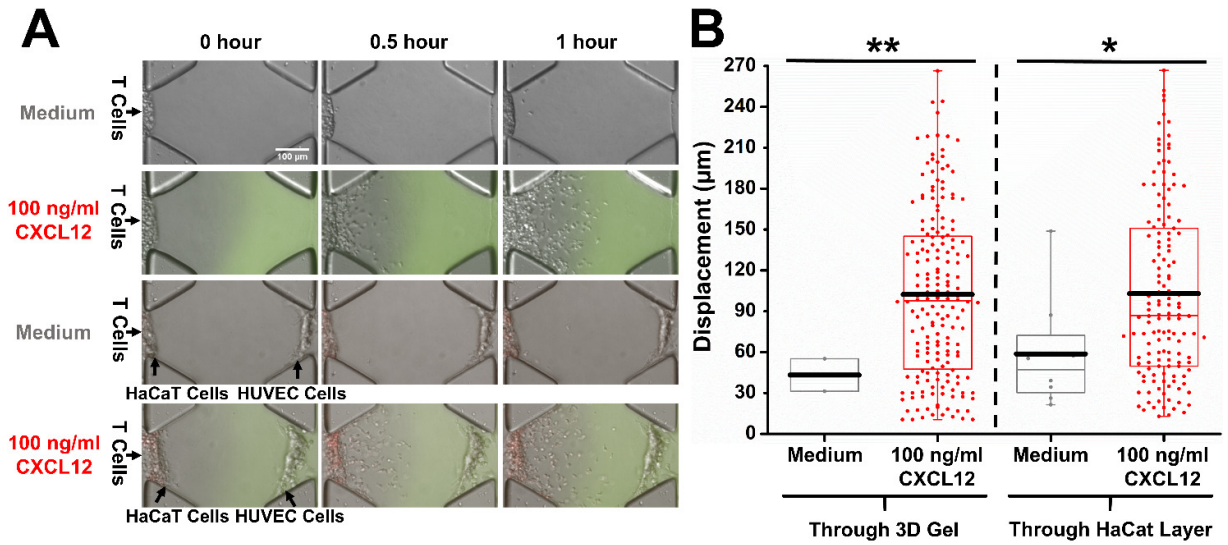

Figure 3. CXCL12 induced T cell migration through a HaCaT cell layer or collagen gel layer in the SoC model. (A) Representative images of T cell transmigration through a HaCaT cell layer or collagen gel layer in the presence of a CXCL12 gradient and medium control conditions in the microfluidic device at 0h, 0.5h, and 1h, respectively (scale bar: 100 µm). The red colored dots in the images show the labelled T cells; the green color in the images indicates the profile and most concentrated area of the CXCL12 gradient. **(B)** The displacement analysis of T cells in different experimental groups at 1h from Figure A. The box charts show the total displacement of individual T cells in the corresponding experimental groups in Figure A; the top and bottom of the whisker show the maximum and minimum values; the box includes the migrated T cells within the range from 25% - 75% of total cells based on the ranked displacement value; the black bold line indicates the mean displacement value. The data in different groups were compared using the two sample Student's t-test, significant difference was indicated using *p < 0.05, **p < 0.01, and ***p < 0.001.

In order to validate the SoC model and mimic CXCL12 induced T cell migration during skin inflammation, we challenged T cells to transmigrate through the HaCaT layer in the presence of a gradient of CXCL12 (100 ng/mL), with medium serving as the control. Labelled T cells were loaded into the channel to demonstrate the integrity of a leakage-free gel. These experiments excluded possible T cell leakage from the collagen gel at the start of experiment (0h). We showed that 18 fold increase in T cells transmigrating through the HaCaT layer towards the CXCL12 gradient with significantly higher mean cell displacement compared to the medium control, which is consistent with the known CXCL12 effect of inducing T cell chemotaxis (**Figure 3**). Considering the clear size and morphology difference between T cells and HUVEC & HaCaT cells, migrating T cells in the collagen gel channel can be easily distinguished without labelling. We tested the migration of T cells through the collagen gel alone (without HaCat layer) under the same conditions (i.e., 100 ng/mL of CXCL12 and medium control) to assess whether absence of a HaCaT layer could affect T cell migratory behavior. Irrespective of the HaCat layer, we found that more than 61 fold increase of T cells transmigrating through the 3D collagen gel layer towards

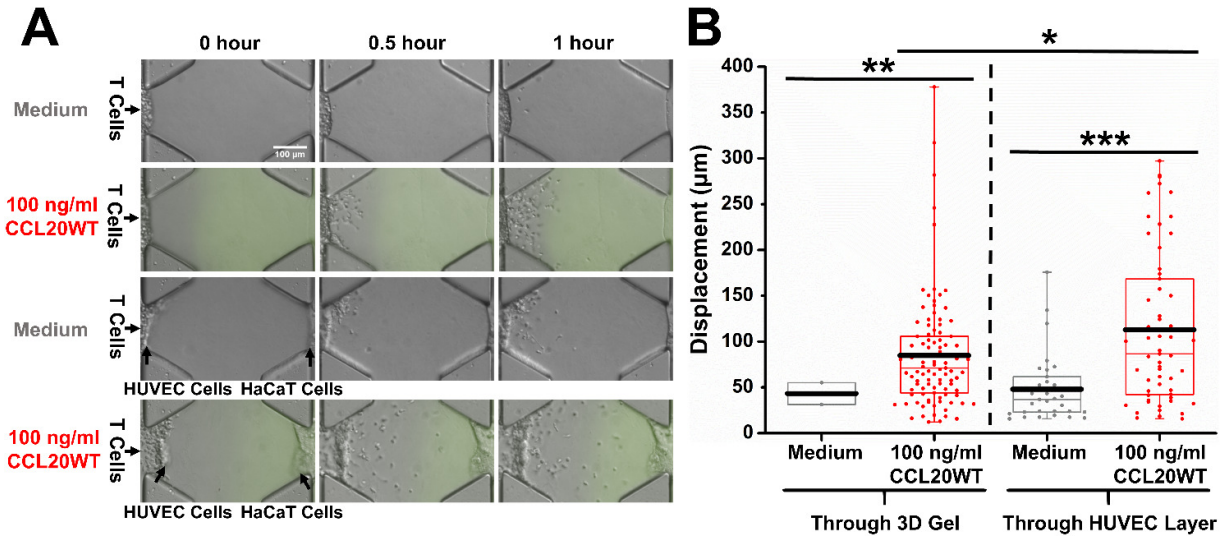

Figure 4. CCL20 induced T cell migration through a HUVEC cell layer or collagen gel layer in the SoC model. (A) Representative images of T cell transmigration through a HUVEC cell layer or collagen gel layer in a CCL20WT gradient and medium control in the microfluidic device at 0h, 0.5h, and 1h, respectively (scale bar: 100 µm). The green color in the images indicates the profile and most concentrated area of CCL20WT gradient. Note that the images of T cell migration through the collagen gel layer in medium control (i.e., the first row of three images) is the same set of experiment shown in Figure 3A. **(B)** The displacement analysis of T cells in different experimental groups is shown at 1h from Figure A. The box charts show the total displacement of individual T cells in the corresponding experimental groups in Figure A; the interpretation of box chart is the same as previously described. The data in different groups were compared using the two sample Student's t-test, significant difference was indicated using *p < 0.05, **p < 0.01, and ***p < 0.001.

the CXCL12 gradient, with significantly higher mean cell displacement compared to the medium control. Hence, we concluded that T cell migration in the presence of the CXCL12 gradient was not impeded by the HaCaT layer (**Figure 3**). In addition to T cells, the device was validated with human blood neutrophils. Our results showed that a gradient of 100 nM (i.e., 43.76 ng/mL) N-formylmethionyl-leucyl-phenylalanine (fMLP) was able to attract neutrophil chemotaxis through collagen gel, while no neutrophils migrated at all in the medium control (**Figure S2**). Our finding is consistent with the literature and our previous results with other microfluidic devices.[48-50]

CCL20 induced T cell migration in the SoC model

To mimic the effects of CCL20 induced cutaneous T cell migration during inflammation, we tested the transmigration behavior of human T cells through a HUVEC layer in a gradient of CCL20WT (100 ng/mL) versus medium control. The CCL20WT gradient induced 1.8 fold increase of T cells transmigrating through the HUVEC layer, with higher mean cell displacement compared to the medium control (**Figure 4**). We then validated T cell migration in collagen gel alone under the same conditions (i.e., 100 ng/mL of CCL20WT and medium control) and tested whether the absence of a HUVEC layer affects the migratory behavior of the T cells. Our results consistently demonstrated that 33 fold increase in T cells transmigrating through the 3D collagen gel layer towards the CCL20WT gradient with significantly higher mean cell displacement compared to the medium control. In addition, the absence of a HUVEC layer significantly reduced the mean displacement of migrated T cells in the CCL20WT gradient as compared to the presence of a HUVEC layer (**Figure 4**).

Effects of co-existing chemokine fields on T cell migration in the SoC model

S1P has been reported to be highly expressed in the skin and blood vessels during cutaneous inflammation.[22] Using a previously designed radial microfluidic device,[45] we performed a quantitative analysis of T cell migration and chemotaxis in medium control and a gradient of S1P at different concentrations in 2D condition. The results obtained from the radial microfluidic device showed that S1P significantly induced T cell chemotaxis at the concentrations of 100 nM (i.e., 37.95 ng/mL), 200 nM (i.e., 75.90 ng/mL), 300 nM (i.e., 113.85 ng/mL) and 500 nM (i.e., 189.75 ng/mL) compared to medium control, with the highest number of migrated T cells at 200 nM and the highest mean cell displacement at 300 nM (**Figure S3**). Thus, we used the range from 200 to 300 nM of S1P as a reference and 100 ng/mL of S1P for cell migration experiments in the SoC model. Skin inflammation requires T cells to navigate a complex chemical cutaneous environment. To determine whether our SoC model can replicate such challenging conditions, we decided to devise an experiment to investigate T cell migration in a microenvironment of competing chemokine gradients. Specifically, gradients of CXCL12 (100 ng/mL) and CCL20WT (100 ng/mL) were generated at the HUVEC side and HaCaT side, respectively, with or without a uniform S1P (100 ng/mL) background, to mimic the complex chemical environment during skin inflammation. We quantified the impact of these SoC conditions for T cell migration. Our results demonstrated the importance of S1P for the outcome of these experiments. Fourteen percent less of T cells transmigrated through the HaCaT layer towards the CXCL12 gradient with significantly lower mean cell displacement in the presence of a uniform S1P background as compared to the absence of S1P (**Figure 5**). We

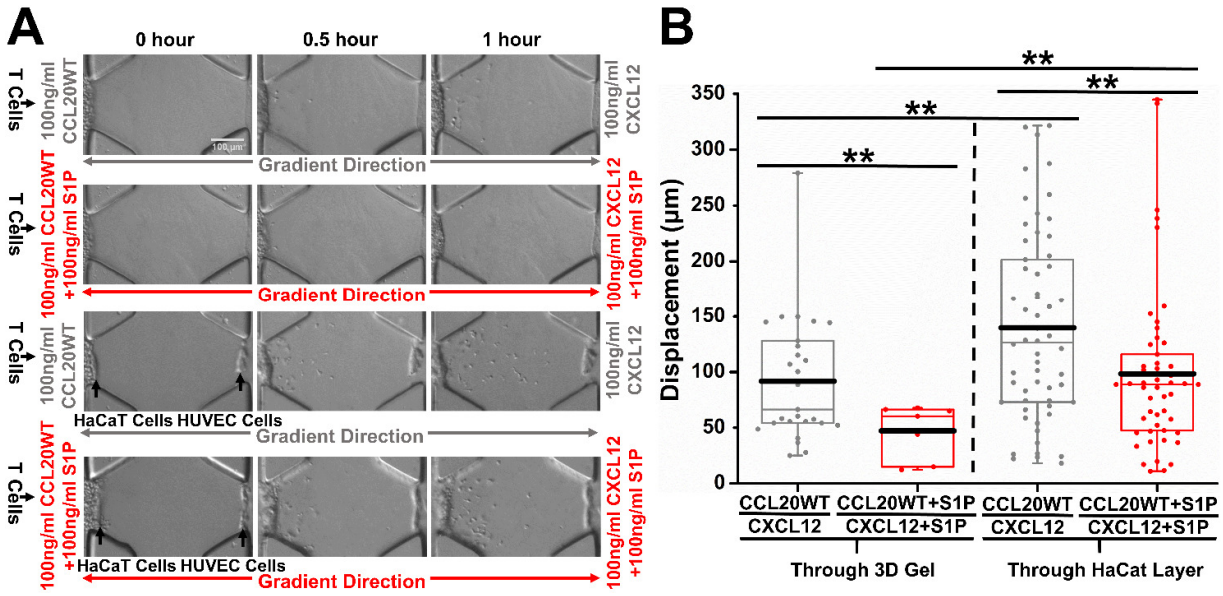

Figure 5. The retention effect of S1P on T cell migration in co-existing chemokine fields in the SoC model. (A) Representative images of T cell transmigration through a HaCaT cell layer or collagen gel layer in different competing gradient groups in the microfluidic device at 0h, 0.5h, and 1h, respectively (scale bar: 100 μm). **(B)** The displacement analysis of T cells in different experimental groups at 1h from Figure A. The box charts show the total displacement of individual T cells in the corresponding experimental groups in Figure A; the interpretation of box chart is the same as previously described. The data in different groups were compared using the two sample Student's t-test, significant difference was indicated using *p < 0.05, **p < 0.01, and ***p < 0.001.

further investigated T cell migration in the collagen gel alone under the same conditions (i.e., CXCL12 gradient at the HUVEC side and CCL20WT gradient at HaCaT side, with and without uniform S1P background) and tested whether the absence of a HaCaT layer could affect T cell migratory behavior. Again, one quarter of T cells transmigrated through collagen gel layer towards the CXCL12 gradient with significantly lower mean cell displacement in the presence of a uniform S1P background as compared to a lack of S1P background. Moreover, the absence of the HaCaT layer resulted in fewer T cells transmigrating towards the CXCL12 gradient and significantly lower mean cell displacement in the same competing gradients with or without S1P when compared to the HaCaT layer being present (**Figure 5**).

CCL20LD inhibits T cell migration in the SoC model

In cell based assays, CCL20LD is an effective inhibitor of CCR6-mediated cell migration and can prophylactically inhibit T cell-associated skin inflammation in animal models of psoriasis.[18] We wanted to test whether CCL20LD can disrupt CCR6/CCL20 receptor-ligand interaction and negatively affect T cell migration in our SoC model. We first examined T cell transmigration through a HUVEC layer in a gradient of CCL20LD (100 ng/mL) or a gradient of CCL20WT (100 ng/mL) with a coexisting uniform CCL20LD (1.6 μg/mL). Results were compared with those of T cell migration in a gradient of CCL20WT (100 ng/mL) or medium control in the SoC model. Around 2 fold increase of T cells transmigrating through the HUVEC layer in the CCL20WT gradient, with significantly higher mean cell displacement when compared to both CCL20LD and medium control conditions. This CCL20WT induced T cell migration was significantly muted by a coexisting uniform CCL20LD background and resulted in less than half of T cells transmigrating through the HUVEC layer and significantly lower mean cell displacement (**Figure 6**). To investigate this further, we studied the CCL20LD inhibitory effect on CCR6-mediated T cell migration in collagen gel alone under the same conditions to test whether the absence of the HUVEC layer can alter the T cell migratory response. Consistently, the CCL20WT gradient attracted 4 fold and 33 fold the number of T cells through the collagen gel layer compared to the CCL20LD gradient and medium control, respectively. This migratory response was completely blocked in the presence of a coexisting uniform CCL20LD. Under the same conditions, the absence of HUVEC layer did not significantly affect T cell migration except for the CCL20WT group, which showed fewer migrated T cells with significantly reduced mean cell displacement when compared to the presence of a HUVEC layer (**Figure 6**).

TNF-α induced cutaneous inflammation in the SoC model

We wanted to examine whether TNF-α stimulation can be used to reconstitute skin inflammation *in vitro* in our SoC model. First, TNF-α stimulation was conducted in the SoC model and, upon stimulation, supernatants were collected as described in the method section. T cell transmigration though

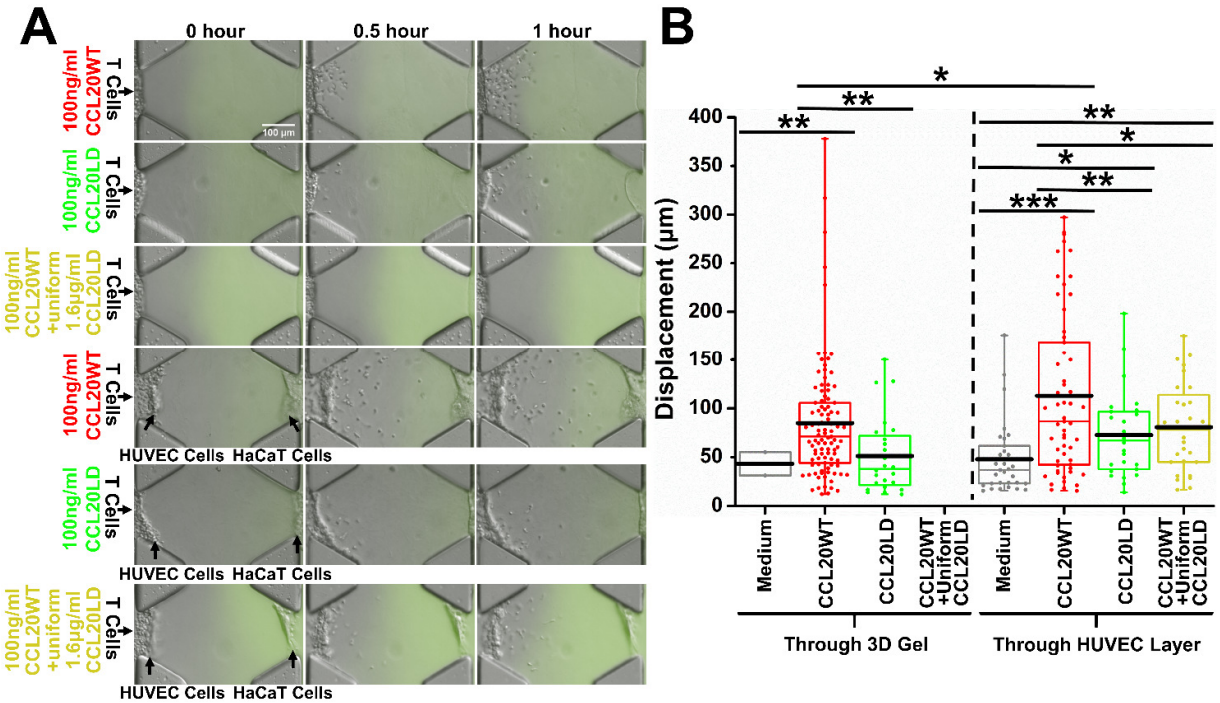

Figure 6. The inhibitory effect of CCL20LD on T cell migration through a HUVEC cell layer or collagen gel layer in the SoC model. (A) Representative images of T cell transmigration through a HUVEC cell layer or collagen gel layer in different groups in the microfluidic device at 0h, 0.5h, and 1h, respectively (scale bar: 100 μm). The green color in the images indicates the profile and most concentrated area of each gradient. Note that the images of T cell migration in CCL20WT gradient (i.e., the first and fourth rows of the images) are the same sets of experiments shown in Figure 4A. **(B)** The displacement analysis of T cells in different experimental groups at 1h from Figure A. Note that the data in the "Medium" and "CCL20WT" groups used for comparison were from the same set of experiments shown in Figure 4B. The colored box charts show the total displacement of individual T cells in the corresponding experimental groups in Figure A; the interpretation of box chart is the same as previously described. Note that no T cells transmigrated through the collagen gel layer in the "CCL20WT+Uniform CCL20LD" group. The data in different groups were compared using the two sample Student's t-test, significant difference was indicated using *$p < 0.05$, **$p < 0.01$, and ***$p < 0.001$.

a HUVEC layer was tested in a gradient of collected supernatants with or without a coexisting gradient of CCL20LD (100 ng/mL) applied in the same direction and all results were compared to the medium control. T cell transmigration through the HUVEC layer towards the gradient of supernatants was significantly enhanced, with one-third more migrated T cells showing significantly higher mean cell displacement compared to medium control (**Figure 7**). This positive effect of the supernatants on T cell migration was not significantly reduced in the presence of a coexisting gradient of CCL20LD in the SoC model (**Figure 7**).

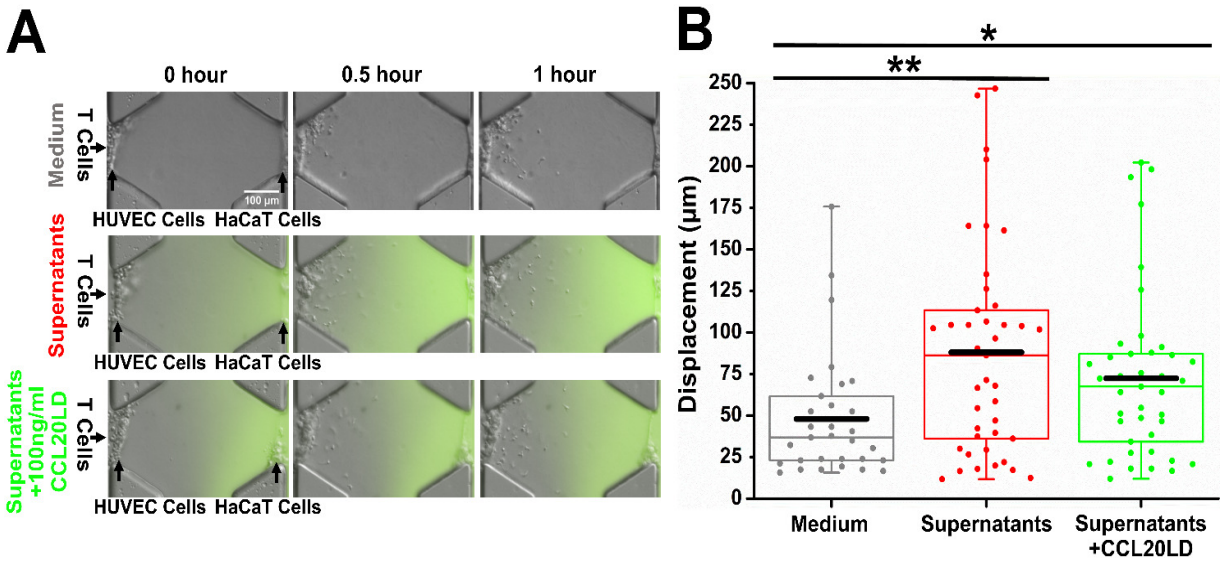

Figure 7. Supernatants from TNF-α stimulation induced T cell migration through a HUVEC cell layer in the SoC model. (A) Representative images of T cell transmigration through a HUVEC cell layer in the medium control and two supernatants groups in the SoC model at 0h, 0.5h, and 1h, respectively (scale bar: 100 µm). The green color in the images indicates the profile and most concentrated area of the gradient. Note that the images of T cell migration in medium control (i.e., the first row of three images) is the same set of experiments shown in Figure 4A. **(B)** The displacement analysis of T cells in different experimental groups at 1h from Figure A. The colored box charts show the total displacement of individual T cells in the corresponding experimental groups in Figure A; the interpretation of box chart is the same as previously described. The data in different groups were compared using the two sample Student's t-test, significant difference was indicated using *p < 0.05, **p < 0.01, and ***p < 0.001.

Discussion

Defined gel pattering in a microfluidic device enables the precise separation of cellular components and the formation of multiple chemical gradients with controllable directional flows. These are critical parameters in designing a sophisticated 3D tissue microenvironment that permits a quantifiable assessment on the migratory behaviors of immune cells. To this end, many studies have been using pillar-like designs in their devices for precise gel pattering.[36-39] Huang et al. developed a microfluidic device with post arrays resulting in multiple discrete 3D cell-laden hydrogel pattering for multicellular co-cultures.[36] Del Amo and coworkers developed a microfluidic device that applied micro-columns with surface tension in the channels for selective gel pattering to quantitatively study 3D chemotaxis of dermal human fibroblasts across the interface of collagen gel-based ECM in response to different chemoattractants.[38] To improve the complexity of the 3D system and to address limitations in the lack of cell-cell interactions for cell migration, Han et al. effectively integrated ECM, chemical gradient, and multicellular co-cultures in a microfluidic device for neutrophil transendothelial migration (TEM).[37] This device mainly consists of one middle endothelial (EC) channel, two chemical side channels, and four smaller "T-shaped" ECM channels. The four ECM channels were designed in symmetry and each of them was flanked by one EC channel and one side channel. By using the similar pillar-like design for the microfluidic device, selective gel pattering was achieved for TEM in precisely configured 3D microenvironments. Similarly, Wu and coworkers developed a microfluidic device for the study of *in vivo*-like neutrophil TEM.[39] This device is composed of one top gel channel, two symmetric "V-shaped" side channels, and one "V-shaped" bottom channel, all internally connected with a central gel chamber. The presence of pillars in the gel chamber applied with surface tension enabled a precise configuration of ECM, EC, and chemical gradient generation for the relevant investigations.

Although the principle of using micropillars for selective gel patterning is not new,[36-39] our SoC model includes innovative and compact micropillar design as reflected by their number, layout, and dimensions within the device. The major gel compartment of our design is 500 µm wide and contains four trapezoidal micropillars which are separated from each other by a 120 µm gap. Many studies applied gel compartments in macroscale (e.g., ≥ 800 µm) to increase the ratio of gap-to-compartment width in an attempt to reduce the risk of gel leakage.[37, 38] In addition, the device size is frequently compromised by the length of major compartment that is composed of numerous micropillars in these studies, restricting the use of the device to one experiment performed

each time.[36-38] By contrast, our device is designed with fewer micropillars and reduced compartment length (1140 µm), provides multiple fields of view for monitoring cell migration, and enables four independent experiments to be conducted simultaneously on a single device to expedite statistically validated experimental throughput. Furthermore, all these mentioned studies did not include the epidermal skin layer but only included ECM and endothelial cells, thus, providing an incomplete reconstruction of the skin *in-vivo* microenvironment.[36-39] Contractively, our device enables us to reconstitute key components of the human skin, including epidermis, dermis, and hypodermis in a well-controlled manner. Our SoC model is a promising in-vitro platform that not only integrates key features of human skin composed by relevant human cells and ECM but enables the reconstitution of complex chemical fields during skin inflammation generated by a single or co-existing chemical gradients and allows direct image analysis of T cell migration in a close to physiological 3D microenvironment.

Our unique SoC model provided new insight into T cell migratory behavior in a spatial cell-matrix composition that mimics aspects of skin inflammation to investigate the effect of individual cellular component. Validation of relevant chemokines (i.e., CXCL12 and CCL20) in our SoC model confirmed previous studies and replicated CXCL12 induced T cell transmigration from the epidermis to dermis and hypodermis for inflammatory angiogenesis,[19-21] and CCL20 mediated T cell transmigration to the inflammatory sites from the hypodermis.[8, 18] A single gradient of CXCL12 or CCL20WT significantly promoted T cell transmigration in our SoC model. The presence of a HUVEC cell layer promoted T cell migration, as shown by a significantly higher mean T cell displacement towards the CCL20WT gradient when compared to a setup devoid of HUVEC cell layer. This suggests that cellular interactions are important for T cell migration. The importance of ECM and 3D organization in our SoC model for T cell migration became obvious when comparing data obtained with this 3D device and 2D systems. Using our previously designed microfluidic device (i.e., the D^3-Chip),[42, 44] very poor or different migratory responses of T cells were observed in 2D condition compared to the 3D conditions (i.e., SoC model). Contrary to the results obtained with the 3D SoC device, our results in the 2D system showed that low numbers of T cells migrated to the gradient of 1 µg/mL CCL20WT with mean cell displacement values comparable to medium control. At identical concentrations (i.e., 1 µg/mL, 10 µg/mL, and 100 µg/mL), CCL20WT and CCL20LD had similar effect on T cell migration, as shown by comparable migrated T cell numbers and mean cell displacement values (**Figure S4**). Also, CCR6 expression of ahPBTs in the flow cytometry analysis (21.8%) and 2D on-chip staining (i.e., on-chip staining of T cells on top of the collagen substrate after cell migration experiments) was relatively low when compared to the 3D condition (i.e., on-chip staining of T cells within collagen gel after cell migration experiments) (**Figures S5**). These results demonstrated that the transmigrated T cells in collagen gel were CCR6 positive. The superiority of 3D systems over 2D systems in predicting cell migratory responses has previously been reported and likely result from improved reconstitution of a more physiological tissue microenvironment.[29, 36]

The SoC model provides a controlled microenvironment in which to simulate complex cytokine gradients that mediate T cell migration during skin inflammation. T cell trafficking from secondary lymphoid tissues via the blood stream to the different skin layers during cutaneous inflammation is a highly dynamic process and engages multiple chemotactic signaling pathways.[8, 51, 52] For example, down-regulation of the lymph node homing receptor CCR7 and its ligands CCL21/19 coincides with an up-regulation of the CCR6/ CCL20 axis in the dermis and epidermis during cutaneous inflammation. This facilitates the egress of T cells from regional lymph nodes to the blood stream and transmigration of T cells from blood vessels to the inflammatory skin sites as part of the specific immune response.[8] The up-regulation of the CXCXR4/ CXCL12 axis in the hypodermis during skin inflammation results in reversed T cell trafficking to the sites of inflammatory angiogenesis.[19-21] Detailed studies demonstrated the up-regulation of the S1PR1/ S1P system in inflamed peripheral tissues (i.e., skin and blood vessels) and its high expression at inflammatory sites is believed to contribute to local T cell retention.[22] We tested the migratory responses of T cells in a set of competing gradient experiments. This included T cell migration in a co-existing gradient of CXCL12 and CCL20WT at the HUVEC side and HaCaT side, respectively, with or without a uniform S1P background. The presence of a uniform S1P background significantly muted T cell transmigration through the HaCaT layer towards a CXCL12 gradient, which was consistent with previous reports that identified high expression of S1P as a retention signal for T cells at inflammatory sites.[22] Cell-cell interactions may promote T cell migration since we found a consistent impairment in T cell migration in the absence of HaCaT cell layer in the same competing gradient experiments. These results demonstrated a strength of the SoC model in monitoring and quantifying migration parameters of individual T cells in complex *in-vivo* chemical fields and the potential for the discovery of relevant chemotactic signaling pathways as new therapeutic targets. Significant involvement of additional chemotactic signaling pathways, including CCR4/ CCL17 and CCR10/ CCL27, have been identified in cutaneous inflammation,[51, 52] and the SoC model is a suitable platform to study their role in cutaneous T cell migration. Another strength of our multicellular SoC model is the ability to collect conditioned flow-through media to reconstitute skin inflammation intrinsically using specific TNF-α stimulation. Supernatants from TNF-α treated HaCaT cells applied to the SoC device revealed a significantly enhanced T cell transmigration through the HUVEC cell layer towards the gradient with significantly higher mean cell displacement compared to medium control conditions. These T cell migratory responses under conditions of complex pro-inflammatory stimuli is consistent with reports of different

pro-inflammatory mediators capable of attracting T cells during skin inflammation.[8, 18-22, 35]

The emergence of increasingly sophisticated "organ-on-chip" devices that utilize human cells in 3D matrices has made this strategy a viable alternative to animal experimentation for cell migration and drug screening studies.[29, 35, 53] The importance of T cell migration for maintaining skin homeostasis and the impact of dysregulated chemotactic signaling pathways on the pathogenesis of various skin diseases has been recognized.[9-13, 52] The development of new immunotherapeutics targeting T cell chemotaxis for the treatment of a broad range of skin diseases has been realized,[51, 52] and requires advanced microfluidic devices capable of adequately simulating specific tissue microenvironmental cues. T cell homing to psoriatic inflammatory sites coincides with an upregulation of the CCR6/ CCL20 axis in the dermis and epidermis,[8, 18] and this CCR6-mediated T cell migration can be muted by an engineered CCL20LD inhibitor believed to be a promising immunotherapeutic for the treatment of psoriasis.[18] With our SoC model, we were able to demonstrate that a uniform background of CCL20LD peptide disrupted T cell migration towards the CCL20 gradient. Furthermore, the SoC device also revealed the dominant pro-migratory effect of supernatants from TNF-α stimulated HaCaT cells on T cell migration in the presence of a co-existing gradient of CCL20LD. This finding is consistent with a previous report that demonstrated a marginal impact of CCL20LD on other chemokine receptor signaling.[18] Collectively, the knowledge gained from applications of skin disease-relevant inhibitors, like CCL20LD, in this new SoC microfluidic model identifies this device as a versatile new chemotactic drug screening tool capable of providing mechanistic insight vital for improving the design and therapeutic application of innovative immunotherapeutics.

Despite of the advantages of our SoC model for T cell transmigration, some limitations should be considered in future development. The use of HaCaT/ HUVEC cells and 3D collagen gel to mimic the key features of different cutaneous compartments are much simplified compared to the complex *in-vivo* conditions. In addition, gradient control in collagen gel is not as accurate and flexible compared with the flow-based 2D microfluidic systems. Furthermore, collagen gel is mechanically sensitive to cell attachment and transmigration and is unstable over long time, which can affect the gel-cell interface, ECM stability and gradient generation. In this direction, other hydrogels such as gelatin methacrylamide (GelMA) with tunable mechanical and biological properties can be considered as alternatives to mimic the ECM in the SoC model,[54] which is especially useful for studying long-time psoriasis tissue formation mediated by T cell migration.

Conclusions

We introduce a SoC model of reconstituted cutaneous microenvironment *in vitro*. This novel microfluidic device allowed us, for the first time, to quantitatively analyze human T cell migration in a multicellular 3D environment under controlled single and competing chemical gradient conditions. We demonstrate the feasibility and potential of this SoC model as a new medium throughput discovery and screening tool to study the involvement of T cell trafficking in complex chemical fields during cytokine-stimulated skin inflammation.

Author Contributions

X.O. Ren and F. Lin conceived and designed the experiments; A. E. Getschman, B. F. Volkman, T. Klonisch, D. Levin, S. Hwang, M. Zhao, S. Santos, and S. Liu contributed reagents, materials and research discussion; X.O. Ren performed the research and analyzed the data; J. Cheng assisted the T cell migration experiments at different concentrations of S1P in the radial microfluidic device; F. Lin supervised the study; X.O. Ren wrote the first draft of the manuscript; all the authors edited the manuscript.

Conflicts of interest

There are no conflicts to declare.

Acknowledgements

This work is financially supported by a Discovery Grant from the Natural Sciences and Engineering Research Council of Canada (NSERC) (RGPIN-2014-04789) to F. Lin. X.O. Ren thanks the Graduate Enhancement of Tri-Council Stipends (GETS) program at the University of Manitoba for financial support. A. E. Getschman thanks the financial support of an Early Career Research Award from the National Psoriasis Foundation. B. F. Volkman thanks the financial support of a Translation Research Award from the National Psoriasis Foundation. T. Klonisch is grateful to the Natural Sciences and Engineering Research Council of Canada (NSERC) for funding. We thank the Nano-Systems Fabrication Laboratory at the University of Manitoba for their technical support. We also thank the Victoria General Hospital in Winnipeg for managing blood samples.

References

1. K. L. Medina, in *Handbook of Clinical Neurology*, eds. J. P. Sean and V. Angela, Elsevier, 2016, vol. Volume 133, pp. 61-76.
2. K. Reif, E. H. Ekland, L. Ohl, H. Nakano, M. Lipp, R. Forster and J. G. Cyster, *Nature*, 2002, **416**, 94-99.
3. S. Hardtke, L. Ohl and R. Förster, *Blood*, 2005, **106**, 1924.
4. C. Otero, M. Groettrup and D. F. Legler, *The Journal of Immunology*, 2006, **177**, 2314-2323.
5. R. Forster, A. C. Davalos-Misslitz and A. Rot, *Nature reviews. Immunology*, 2008, **8**, 362-371.
6. S. Nandagopal, D. Wu and F. Lin, *PloS one*, 2011, **6**, e18183.
7. L. Dupre, R. Houmadi, C. Tang and J. Rey-Barroso, *Frontiers in immunology*, 2015, **6**, 586.
8. C. Brinkman, J. Peske and V. Engelhard, *Frontiers in immunology*, 2013, **4**.

9. M. Vičić, S. Peternel, E. Simonić, V. Sotošek-Tokmadžić, D. Massari, I. Brajac, M. Kaštelan and L. Prpić-Massari, *Medical Hypotheses*, 2015, **87**, 66-68.
10. K. Shams, G. J. Wilson, M. Singh, E. H. van den Bogaard, M. L. Le Brocq, S. Holmes, J. Schalkwijk, A. D. Burden, C. S. McKimmie and G. J. Graham, *The Journal of Investigative Dermatology*, 2017, **137**, 85-94.
11. M. Jang, H. Kim, Y. Kim, J. Choi, J. Jeon, Y. Hwang, J. S. Kang and W. J. Lee, *Experimental dermatology*, 2016, **25**, 598-603.
12. Z. Dai, L. Xing, J. Cerise, E. H. C. Wang, A. Jabbari, A. de Jong, L. Petukhova, A. M. Christiano and R. Clynes, *The Journal of Immunology*, 2016, **197**, 1089-1099.
13. S. Li, G. Zhu, Y. Yang, Z. Jian, S. Guo, W. Dai, Q. Shi, R. Ge, J. Ma, L. Liu, K. Li, Q. Luan, G. Wang, T. Gao and C. Li, *Journal of Allergy and Clinical Immunology*, 2016.
14. L. Ventrelli, L. Marsilio Strambini and G. Barillaro, *Advanced Healthcare Materials*, 2015, **4**, 2606-2640.
15. N. H. Nicol, *Dermatology nursing*, 2005, **17**, 62.
16. P. A. J. Kolarsick, M. A. Kolarsick and C. Goodwin, *Journal of the Dermatology Nurses' Association*, 2011, **3**.
17. C. M. A. Reijnders, A. van Lier, S. Roffel, D. Kramer, R. J. Scheper and S. Gibbs, *Tissue engineering. Part A*, 2015, **21**, 2448-2459.
18. A. E. Getschman, Y. Imai, O. Larsen, F. C. Peterson, X. Wu, M. M. Rosenkilde, S. T. Hwang and B. F. Volkman, *Proc Natl Acad Sci U S A*, 2017, **114**, 12460-12465.
19. M. J. del Rey, E. Izquierdo, S. Caja, A. Usategui, B. Santiago, M. Galindo and J. L. Pablos, *Arthritis & Rheumatism*, 2009, **60**, 2926-2934.
20. E. R. Fedyk, D. Jones, H. O. D. Critchley, R. P. Phipps, T. M. Blieden and T. A. Springer, *The Journal of Immunology*, 2001, **166**, 5749.
21. S. Zgraggen, R. Huggenberger, K. Kerl and M. Detmar, *PloS one*, 2014, **9**, e93665-e93665.
22. M. Aoki, H. Aoki, R. Ramanathan, N. C. Hait and K. Takabe, *Mediators of Inflammation*, 2016, **2016**, 8606878.
23. A. D. van der Meer, A. A. Poot, M. H. G. Duits, J. Feijen and I. Vermes, *Journal of Biomedicine and Biotechnology*, 2009, **2009**, 823148.
24. G. Velve-Casquillas, M. Le Berre, M. Piel and P. T. Tran, *Nano today*, 2010, **5**, 28-47.
25. F. Lin and E. C. Butcher, *Lab on a Chip*, 2006, **6**, 1462-1469.
26. F. Lin, in *Methods in Enzymology*, Academic Press, 2009, vol. Volume 461, pp. 333-347.
27. J. Li and F. Lin, *Trends in Cell Biology*, 2011, **21**, 489-497.
28. J. Wu, X. Wu and F. Lin, *Lab on a Chip*, 2013, **13**, 2484-2499.
29. X. Ren, D. Levin and F. Lin, *Micromachines*, 2017, **8**, 324.
30. S. Y. Chang, E. J. Weber, K. P. V. Ness, D. L. Eaton and E. J. Kelly, *Clinical Pharmacology & Therapeutics*, 2016, **100**, 464-478.
31. B. R. Ware and S. R. Khetani, *Trends in Biotechnology*, 2016, **35**, 172-183.
32. T. T. G. Nieskens and M. J. Wilmer, *European Journal of Pharmacology*, 2016, **790**, 46-56.
33. R. Visone, M. Gilardi, A. Marsano, M. Rasponi, S. Bersini and M. Moretti, *Molecules*, 2016, **21**.
34. P. Moura Rosa, N. Gopalakrishnan, H. Ibrahim, M. Haug and O. Halaas, *Lab on a Chip*, 2016, **16**, 3728-3740.
35. M. Wufuer, G. Lee, W. Hur, B. Jeon, B. J. Kim, T. H. Choi and S. Lee, *Sci Rep*, 2016, **6**, 37471.
36. C. P. Huang, J. Lu, H. Seon, A. P. Lee, L. A. Flanagan, H.-Y. Kim, A. J. Putnam and N. L. Jeon, *Lab on a chip*, 2009, **9**, 1740-1748.
37. S. Han, J.-J. Yan, Y. Shin, J. J. Jeon, J. Won, H. Eun Jeong, R. D. Kamm, Y.-J. Kim and S. Chung, *Lab on a Chip*, 2012, **12**, 3861-3865.
38. C. Del Amo, C. Borau, N. Movilla, J. Asin and J. M. Garcia-Aznar, *Integrative Biology*, 2017.
39. X. Wu, M. A. Newbold and C. L. Haynes, *Analyst*, 2015, **140**, 5055-5064.
40. K. Chopra, D. Calva, M. Sosin, K. K. Tadisina, A. Banda, C. De La Cruz, M. R. Chaudhry, T. Legesse, C. B. Drachenberg, P. N. Manson and M. R. Christy, *Aesthetic surgery journal*, 2015, **35**, 1007-1013.
41. S. Usami, M. Okazaki, T. Nitta, N. Uemura, T. Homma and K. Akita, *Journal of plastic surgery and hand surgery*, 2017, **51**, 182-186.
42. X. Ren, J. Wu, D. Levin, S. Santos, R. L. de Faria, M. Zhang and F. Lin, *Annals of the New York Academy of Sciences*, 2019, **1445**, 52-61.
43. X. Ren, J. Wu, D. Levin, S. Santos, R. L. de Faria, M. Zhang and F. Lin, *Annals of the New York Academy of Sciences*, 2019, **0**.
44. X. Ren, A. Alamri, J. Hipolito, F. Lin and S. K. P. Kung, in *Methods in Enzymology*, Academic Press, 2019.
45. J. Wu, A. Kumar-Kanojia, S. Hombach-Klonisch, T. Klonisch and F. Lin, *Lab on a Chip*, 2018, **18**, 3855-3864.
46. K. M. Blum, T. Novak, L. Watkins, C. P. Neu, J. M. Wallace, Z. R. Bart and S. L. Voytik-Harbin, *Biomaterials science*, 2016, **4**, 711-723.
47. M. Keating, A. Kurup, M. Alvarez-Elizondo, A. J. Levine and E. Botvinick, *Acta Biomaterialia*, 2017, **57**, 304-312.
48. J. Wu, C. Hillier, P. Komenda, R. L. de Faria, S. Santos, D. Levin, M. Zhang and F. Lin, *Technology*, 2016, **4**, 104-109.
49. K. Yang, J. Wu, L. Zhu, Y. Liu, M. Zhang and F. Lin, *Journal of visualized experiments : JoVE*, 2017, 10.3791/55615.
50. K. Yang, H. Peretz-Soroka, J. Wu, L. Zhu, X. Cui, M. Zhang, C. Rigatto, Y. Liu and F. Lin, *Scientific Reports*, 2017, **7**, 3100.
51. J. W. Griffith and A. D. Luster, *European Journal of Immunology*, 2013, **43**, 1430-1435.
52. F. Lafouresse and J. R. Groom, *Frontiers in immunology*, 2018, **9**.
53. C. Mondadori, M. Crippa, M. Moretti, C. Candrian, S. Lopa and C. Arrigoni, *Frontiers in Bioengineering and Biotechnology*, 2020, **8**.
54. X. Zhao, Q. Lang, L. Yildirimer, Z. Y. Lin, W. Cui, N. Annabi, K. W. Ng, M. R. Dokmeci, A. M. Ghaemmaghami and A. Khademhosseini, *Advanced healthcare materials*, 2016, **5**, 108-118.

